Journal of Materials Chemistry

View Online
Dynamic Article Links

Cite this: DOI: 10.1039/c1jm12829a

www.rsc.org/materials

PAPER

Metal free, end-opened, selective nitrogen-doped vertically aligned carbon nanotubes by a single step *in situ* low energy plasma process†

Ganjigunte R. S. Iyer‡* and Paul D. Maguire

Received 20th June 2011, Accepted 20th August 2011
DOI: 10.1039/c1jm12829a

We report a novel single step *in situ* process of growth and nitrogen-electron cyclotron resonance plasma treatment of vertically aligned multi walled carbon nanotubes (VA-MWCNTs) that leads to concurrent end opening by metal cap removal, nitrogen incorporation and intercalation along with substitution at graphitic sites resulting in n-type electronic doping. Microscopic and spectroscopic evaluations of the nitrogen treated MWCNTs reveal negligible iron content with significant conservation of both structure and alignment. The nitrogen induced electronic change increases distinct π^* states as evidenced by Near Edge X-ray Absorption Fine Structure (NEXAFS) and 5 cm^{-1} downshift of G-band, as observed from Raman spectroscopy, confirm n-type doping. The combined effect of plasma activation (both cavities and surface of the end opened VA-MWCNTs) and n-type doping enhances the field emission performance of the CNTs resulting in high current density (15 mA cm^{-2}) at low applied voltage of 1.5 V μm^{-1} with low turn on and threshold electric fields (E_{to}-0.52 and E_{th}-0.76 V μm^{-1}). This low energy highly controllable plasma has great implications not only in the fabrication of various n-type materials and bio related application but also many other interesting areas for cost effective energy related applications.

Introduction

Carbon nanotubes (CNTs) continue to draw great attention, due to their extraordinary properties over other carbon nanomaterials known to date and are considered as attractive candidates for many diverse nanotechnological applications such as field emission sources, scanning probes, transistors, nanomechanical devices, energy storage, fuel cells, bio (sensors) and molecular electronics *etc.*[1] Of particular interests are the aligned CNTs, with high structural orientation, as they offer unique properties that are highly desired for the integration of nanotubes into many devices. To enable their applications in energy harvesting and sensing devices, it is critical that the nanotubes are of high quality, devoid of any metallic impurities. To control the electronic properties of aligned MWCNTs with specific functional attachment without affecting their physical structure and alignment is of great technological importance.

The synthesis of nanotubes involves exposure of carbonaceous feedstock to a metal catalyst at elevated temperatures. Metal catalysts turn out to be a major impurity if they remain as residues after the CNT synthesis and their removal is imperative to significantly enhance the functionality of these quasi one-dimensional structure in many applications.[1] There have been several approaches, mostly post treatment processes (PTP), for the removal of metal catalyst from the CNTs. However, most of the progress thus far reported has been on the purification of the non-aligned CNTs by chemical PTPs using both covalent and non-covalent functionalisation methods. Traditional wet chemical methods rely on solvents and dispersion of nanotubes, which are known to have considerable impact on the structure and alignment of the nanotubes.[2] The lack of, structural preservation and uniform functionalisation, limits the solution based PTPs for the metal catalyst removal in aligned CNTs. Alternatively, plasma treatments are usually employed to tailor the electronic structures by controlled functionalisation and also, simultaneously, purify them.[3] Plasma has been widely employed as a PTP using various process gases[4–6] and different plasma sources.[7–9] Nitrogen is most commonly chosen for creating n-type CNTs, where the nitrogen atom modifies the electronic structure by creation of donor states near the Fermi level.[10,11] Introduction of nitrogen during the growth process poses a great difficulty of controlling the position of N in the CNT local structure and have shown no signs of metal catalyst removal. Although there have been reports of nitrogen PTPs by other

Nanotechnology and Integrated Bioengineering Centre (NIBEC), School of Electrical and Mechanical Engineering (SEME), University of Ulster, Jordanstown, Shore road, Newtown abbey, County Antrim, BT37 0QB, United Kingdom. E-mail: swathigr@gmail.com; swathi.ganjigunteramaswamy@ndsu.edu; pd.maguire@ulster.ac.uk

† Electronic supplementary information (ESI) available:. See DOI: 10.1039/c1jm12829a

‡ Present address: Materials and Nanotechnology Centre (MNT), Dept. of Physics, South Engineering, Research 1, NDSU Research and Technology Park, P.O. Box 6050, Dept. 2760, Fargo, North Dakota 58108-6050, USA.

plasma techniques for metal catalyst removal and nitrogen doping, they are mostly *ex-situ* process involving the pre-synthesised CNTs which may have been exposed to ambient with possible adsorption of elements, multiple steps or high energy ion bombardment, which is shown to degrade or even destroy the nanotubes.[3–9]

Recently, there has been an overwhelming focus on N-doping of various carbon nanomaterials including graphene for energy storage/conversion devices (Lithium battery application),[12] fuel cells[13–15] and solar cells.[16] Following the pattern, intensive research efforts have emphasised on cost reduction, which is to slowly limit the usage of high cost platinum by replacing it with N-doped carbon materials. Lately, there have been reports of advantages of the metal free vertically aligned nitrogen doped CNTs for oxygen reduction reaction (ORR) with better long-term stability performance than the commercially available platinum electrodes for fuel cell applications.[17,18] In another instance, Ruitao *et al.*, have shown high purity, open ended and well aligned N-doped carbon nanotube- graphene hybrid nanostructures as highly efficient support material for the favourable high performance catalyst support replacing the conventional platinum based support.[19] In this context, drawing motivation from the current trends on developing various n-type carbon nanomaterials for diverse applications, we demonstrate a single step *in situ* process involving, growth and nitrogen plasma treatment of VA-MWCNTs using a conventional microwave plasma enhanced CVD system with a inter-convertible electron cyclotron resonance (ECR) plasma source for high field emission performance, possible bio-sensing, and support material in battery and fuel cell applications.

Experimental

The process of growth and concurrent nitrogen plasma treatment of the aligned CNTs were carried out in a custom built AsTEX Sekitrons's unique flexible inter convertible plasma reactor, where microwave coupling design with static magnetic field (electromagnets) allows plasma processing either in the Microwave Enhanced Chemical Vapour Deposition (MPECVD) mode or microwave assisted Electron Cyclotron Resonance (ECR) mode (Fig. 1). The system consists of a 2.45 GHz, 1.5 kW microwave source with a rectangular wave-guide coupled to the tunable impedance matching network and a quartz window that allows the microwave power into the cylindrical microwave cavity. The chamber is evacuated by a combination of turbo molecular and rotary pump.

Briefly, iron (Fe) catalysts of thickness, 20 nm was sputtered onto silicon substrates using a DC magnetron sputtering system and transferred into the MPECVD system for the CNT synthesis. The samples (Fe coated Si substrates) were then placed on a molybdenum sample holder and mounted on the inductively heated graphite stage, heated *via* a heater control in the chamber and the system was pumped down to base pressure of $\sim 10^{-4}$ Torr. The flow of the feed gases allowed into the chamber through gas distributors, were controlled by the mass flow controllers (MFCs). VA-MWCNTs were synthesised in a gas mixture of methane and nitrogen in the ratio flow rate 20 and 40 sccm respectively, with an input power of 800–850 W, at a substrate temperature of 750 °C, while chamber pressure was maintained at 2×10^{-4} Torr. The growth process was carried for 5 min and the average diameter of these VA-MWCNTs from the SEM were <200 nm.

Further, for the *in situ* plasma treatment of the synthesised nanotubes, the system was allowed to cool down to room temperature and pumped down to 2×10^{-6} Torr and operated in the ECR mode. In the ECR mode, the microwave energy is coupled to the natural resonant frequency of electrons in plasma in the presence of a static magnetic field of 0.0875 T. The resonant frequency occurs when the electron cyclotron frequency matches or equals the excitation frequency. The cyclotron frequency is given as,

$$\omega_{ce} = eB/m_e \quad (1)$$

where e is the charge of the electron, B is the strength of the static magnetic field and m_e is the electronic mass. Low energy

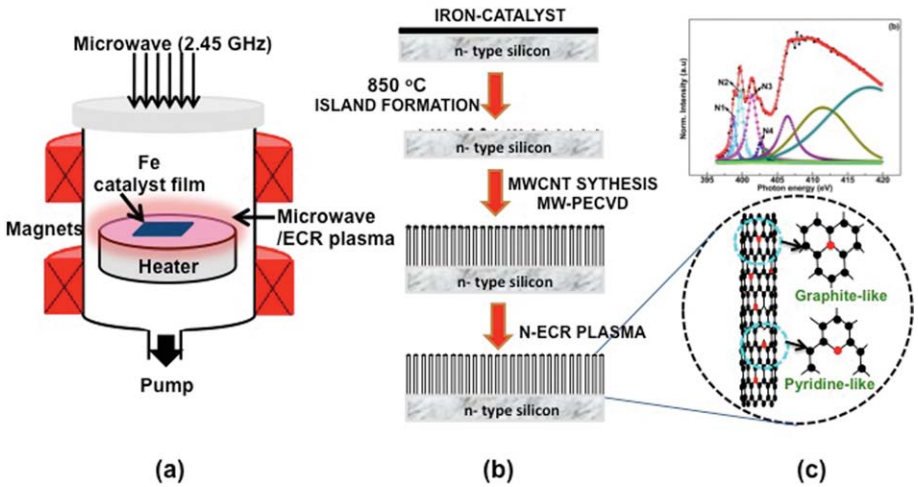

Fig. 1 Schematic illustration of: (a) Microwave Plasma Enhanced Chemical Vapour Deposition (MPECVD) coupled Electron Cyclotron Resonance (ECR) plasma system. (b) Single step process of *in situ* growth (MPECVD) and nitrogen plasma treatment (ECR) of vertically aligned MWCNTs. (c) Local N structure in N-doped MWCNTs.

nitrogen ions, created by the combination of magnetic field and microwave excitation at 100 W were used to treat the VA-MWCNTs for 15 min. The flow rate of the nitrogen was maintained at ~8 sccm and the working pressure of the system during the nitrogen bombardment was 4×10^{-4} Torr. For convenience, the untreated and the nitrogen ECR plasma treated VA-MWCNT samples are referred as UT and N-MWCNTs respectively.

The microstructure and composition of the UT and N-MWCNTs were carried by various microscopic and spectroscopic techniques. The morphology and alignment of the VA-MWCNT films were observed by FEI Quanta Scanning Electron Microscope (SEM). Surface analysis by High Resolution X-Ray Photoelectron Spectroscopy (HR-XPS) was carried out at Daresbury Laboratory using a Scienta ESCA300 spectrometer. The monochromatised Al Kα (1486.7 eV) X-ray source was operated at 2.8 kW (14 kV, 200 mA). Survey scans were recorded at 150 eV pass energy, 1.9 mm slit width, giving an overall instrument resolution of 0.53 eV. Regional spectra were recorded at 150 eV pass energy, 0.5 mm slit width, giving an instrument resolution of 0.35 eV. The samples were mounted on standard stainless steel stubs and introduced to the spectrometer *via* a fast entry air lock and preparation chamber.[20] The pressure in the analysis chamber during XPS analysis was $\sim 10^{-8}$ mbar. Samples were analysed at electron take-off-angles of 90° (relative to the sample surface). A low energy electron flood gun (Scienta FG300) was sometimes used to charge compensate the emitted electron energies, but not during work function measurements. Spectra were quantified using a linear baseline under the core line envelopes and using C 1s, O 1s and other sensitivity factors measured from compounds of known stoichiometry.

The NEXAFS measurements were carried at the Synchrotron Radiation Source (SRS) Daresbury, UK. The sample was fixed on a tantalum sample holder and introduced into the experimental chamber maintained at ultrahigh vacuum. The angle of incidence of the incident X-ray photon with respect to the sample surface normal was fixed at 55 (magic angle = 54.7). Surface sensitive Total-Electron Yield (TEY) mode was used to acquire the data, which were normalised to the signal from the gold-covered grid recorded simultaneously. Carbon *k* edge π^* of graphite, located at 285.35 eV, was used to calibrate the monochromator energy scale. More details on processing of the obtained NEXAFS spectra are described elsewhere.[22] In this paper, we present the interesting changes to the electronic structure of nitrogen ECR treated MWCNTs and it should be mentioned that the ionisation jumps were not considered in this case as in our previous cases of N_2 doped CNTs.[21,22] However, the N–k edge was normalised and fitted by a combination of Lorentzian and Voigt functions as our interest lies in the various π^* resonances, which indicates the evolution of different C–N π^* bonding states in the local structure. Microstructure evaluation was done employing a LabRam 300 micro Raman system using a He–Ne laser (632.8 nm excitation wavelength). All measurements were carried with constant laser power of 3.5 mW and 100× objective from ten different spots of the film sample. The average peak position and intensity ratio (I_D/I_G) values were calculated from the D and G bands peak fitted using a Lorentzian function.

Field emission measurements were carried by a standard parallel plate diode configuration, where the aligned MWCNTs on Si substrate were used as the cathode and a 2 mm tungsten rod as the anode at a base pressure of 10^{-6} mbar. The electrode separation was maintained at 100 μm by a digital micrometre controller and optical microscope. The measurements were carried for both the UT and N-MWCNTs respectively. Finally, we employed static contact angle goniometry (CAM 2000, KSV instruments Ltd., Finland) using de-ionised water by a manual Hamilton 1 ml adjustable precision syringe with proprietary easy to use "One Touch Dispenser" mechanism to study the impact of N-ECR plasma treatment on the wettability of CNT surface.

Results and discussion

Fig. 2(a, b) correspond to the SEM images of UT VA-MWCNTs, while Fig. 2(c, d) to that of N-MWCNTs. It can be seen from the Fig. 2(a, b), that the UT MWCNTs that were closely packed before the plasma treatment are well separated after the N-ECR treatment (Fig. 2(c, d)). The average length of the CNTs was 15 μm, while the average diameter was <200 nm. The nitrogen ion collision, etches away the amorphous carbon encapsulating the CNT surface resulting in well separated tubes (Fig. 2(d, inset (c, d)). It can be seen from Fig. 2(c, d) that the metal catalyst particles capped on the UT MWCNTs are removed leading to end opening after the nitrogen ion bombardment. The structure and alignment of the nanotubes is well preserved after the low energy ion bombardment.

To estimate the efficacy of nitrogen plasma in metal catalyst removal and simultaneous inclusion of nitrogen into the graphitic matrix, elemental analysis by HR-XPS was carried out on both the UT and N-MWCNT samples. Fig. 3(a) shows the wide energy scan (WES) with C 1s at 284.5 eV, N 1s at 400 eV, O 1s at 532 eV and Fe 2p at 730 eV respectively. The elemental

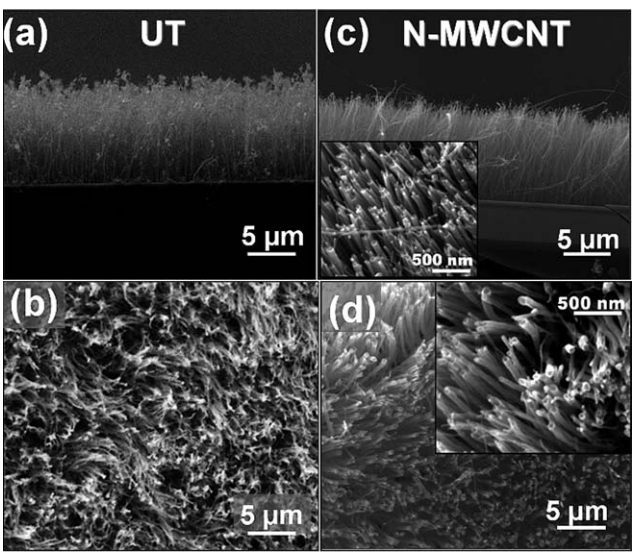

Fig. 2 Scanning electron microscopy (SEM) images of (a, b) UT with the metal catalyst at the top, (c, d) well separated nanotubes with tip opened N-MWCNTs, insets clearly show the tip opening *i.e.* the metal particles are completely removed.

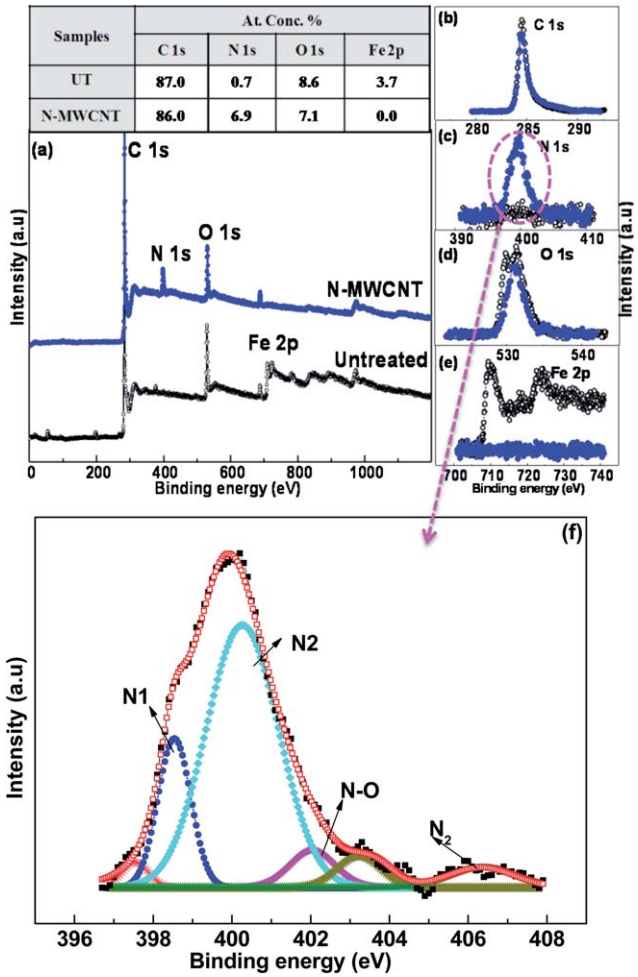

Fig. 3 HR-XPS spectra of UT (open circles) and N-MWCNT (closed circles) samples: (a) wide energy scan (WES) with table containing the atomic concentration of main elements interested and (b, c, d, e) the regional scans of carbon, nitrogen, oxygen and the metal catalyst, iron respectively. 3(f) shows the deconvolution of the N-1s peak.

scans of carbon, nitrogen, oxygen and iron are represented in Fig. 3(b, c, d, e). The prominent Fe 2p double peak present between 710–730 eV (Fig. 3(a, e) in the UT MWCNTs completely disappears after the N-ECR treatment, which corroborates very well with the SEM images of end opened N-MWCNT (Fig. 2 (c, d)). The at % conc. of the Fe 2p decreases from '3.7' to '0' after the N-ECR treatment. The intensity of the carbon peak in the N-MWCNTs is reduced in comparison to the UT nanotubes, which can be due to the amorphous carbon etched along with the metal catalyst particles during the nitrogen ion bombardment (Fig. 3b). Along with metal catalyst removal, the nitrogen ion bombardment also etches away small amounts of amorphous carbon encapsulating the metal catalyst and the CNTs. This indicates that the plasma confinement and ion collisions not only occur on the nanotube tips but also the CNT surface.

To further understand the nitrogen interaction with the graphitic structure, a detailed chemical bonding information was derived from deconvoluting the N 1s peak of the N-MWCNTs (Fig. 3c, blue, closed circles)). Generally, there are several N-moieties or N-functional groups that include pyridinic-N, pyrrolic-N, graphitic-N and N-oxides of pyridinic-N in the nitrogen doped carbon. The deconvolution by Gaussian type of the N 1s, Fig. 3f, reveals significant peaks at 398.4 (±0.2) eV and 400.5 (±0.2) eV accompanied by couple of smaller bands between 402–407 eV respectively. Due to complexity of the assignment of the C–N bonding states, we have considered assignments from our previous work and the assignments from the reports for the CN_x structures that have been widely accepted.[23–28] In case of N-MWCNTs, the low energy component (N1) assigned as the pyridinic-N, refers to nitrogen atom bonded to two sp^2 carbon that is capable of donating one p electron to the aromatic π system. While, the high-energy component (N2) is attributed to the graphite-N or substituted nitrogen, which refers to nitrogen atom incorporated into the graphitic matrix or replacing the carbon atom in the graphitic layer (nitrogen bonded to three sp^2 carbon atom). Two small peaks between 402.3–403.2 eV (±0.4), correspond to the pyridinic-(N^+-O^-) functionalities, where N-oxides of the pyridinic-N are bonded to two carbon atoms and one oxygen atom. Prominent peaks between 405–407 eV are reported to be due to the presence of molecular nitrogen (N_2 gas) trapped inside the tube, due to the end opening (removal of metal catalyst)[29] or nitrogen that is intercalated between the graphitic layers of the CNTs.[28,30–32] The end opening facilitates both incorporation and intercalation of nitrogen (6 at. %) in the CNT structure.

Interestingly, the oxygen concentration in the untreated nanotubes is larger than that in the N-ECR treated samples (Fig. 3d). There can be two possible reasons for the high oxygen concentration in the untreated samples. Firstly, the oxygen may be originating due to the moisture or excess oxygen in the reactor that may be attached to the amorphous carbon in the UT nanotubes. Secondly, soon after the growth process while the sample is still cooling to be further N-ECR plasma treated, the metal catalysts present at the nanotube tip or the amorphous mass remain active. The temperature in the chamber can keep the surface of the metal catalyst active and the Fe particles can possibly undergo oxidation thereby enhancing the concentration of oxygen in the UT nanotubes.[33] The low energy nitrogen ion bombardment using the ECR plasma successfully reduces the oxygen content in the CNT film. We would like to emphasise here that the HR-XPS studies were not *in situ* but carried out long after the plasma treatment, as the measurements were performed at Daresbury facility. Further, the oxygen content in the plasma treated sample can be justified as; the samples soon after plasma treatment have been exposed to the ambient (air), where the activated sites can possibly form oxygen-containing groups. However, the amount of oxygen in the N-ECR treated N-MWCNT is reduced (7.1 at. %) when compared to the UT (8.6 at. %). Compared to some of the reports of nitrogen RF plasma treatment of graphene, including our previous work on aligned MWCNTs, which have resulted in the uptake of oxygen (~40 at. %) mostly from the activated site and defect sites created by the RF plasma,[22] the oxygen content in the N-ECR treated samples is quite low.

NEXAFS is analogous to many other probing techniques particularly, Electron Energy Loss Spectroscopy (EELS), in that the density of unoccupied electronic states of the samples is

achieved by the core level excitation. However, NEXAFS has an upper hand on comparing the spectral resolution, which is 0.1 eV as to 1 eV in EELS and other being, possible destruction to the sensitive samples from the radiation owing to the use of electron beam for excitation in case of EELS unlike soft X-ray in NEXAFS. More importantly, NEXAFS exhibited more structural features, which could not be resolved using EELS. In this case due to the longer probing depth of NEXAFS compared to the surface sensitive XPS method, we have employed NEXAFS to understand and validate the electronic structure of the nitrogen treated MWCNTs from previously obtained methods. Fig. 4(a) presents an overlay of N–K edge NEXAFS spectra of the UT and N-MWCNT at room temperature, while Fig. 4(b) shows the deconvoluted N–K edge of the N-MWCNT. Both spectra exhibited sharp peaks below the ionisation potential of nitrogen corresponding to transitions from 1s into the π^* orbitals and a broad peak from energies 406–420 eV corresponding to the σ^* resonance. The UT N–K edge shows a prominent π^* peak at 400.1 eV and a broad σ^* peak between 406.6–420 eV with no features. The N–K edge of the N-MWCNT shows interesting features after the nitrogen ion bombardment, where the sharp π^* peak splits into three distinct peaks at energies 398.4, 399.5 and 401.5 eV labelled as N1, N2 and N3 respectively. It is very evident that the 1s to π^* transition energy is dependent on the form of nitrogen incorporated in the N-MWCNT. Due to the complexity of the bonding in nitrogenated CNTs there is always difficulty in the assignment of these peaks. In this work we have assigned the peaks in accordance with some of the earlier reports on CN_x films and carbon nanostructures, inclusive of our previous work on nitrogen treated aligned CNTs. As seen in Fig. 4(b), we assign N1 to the pyridinic like nitrogen, N2 to cyanic nitrogen and N3 as related to either graphite like sites or molecular nitrogen.[21,34–36] The peak N3 has a shoulder at 402.4 eV, which may be due to the combined contributions from both N in graphite like sites and molecular N_2.

The low energy π^* band, N1, has nitrogen bonded to two carbon neighbours and appears to be the least intense among the π^* peaks. The pyridine like sites are usually created in the energetic defects created upon chemical/high-energy treatment. Apart from the inherent defect sites in the CNTs, the other possible defects would be those that may have been created by the N-ECR treatment at the tip of the nanotube due to the removal of metal catalyst, which would facilitate the creation of pyridinic like sites. The next intense peak, N2 is attributed to the cyanic like, where a single C–C bond binds the cyanic structure and the basal graphite, which can be imagined to have a standing upright orientation. This represents the nitrogen that is mostly intercalated between the tubes aided by the end opening.[28,30,32] The peak positioned at higher binding energy N3, is the most intense indicating a substantial amount of nitrogen may be present as substitution nitrogen in the hexagonal graphitic structure *i.e.*, nitrogen atoms replace carbon atoms from the six ringed graphite structure and nitrogen is bonded to three carbon atoms in the carbon matrix. Since this π^* band of nitrogen is aligned along the nanotube axis, this localised state can also be indicative of small amounts of molecular nitrogen incorporated within the tube due to the end opening. These vertically aligned end opened nanotubes, grounded to the substrate can be envisaged as end opened test tubes, which can ideally hold incorporated material. In some of the earlier works of nitrogen doped CNTs, the presence of molecular nitrogen encapsulated into the nanotubes is reported to be between 400.8–402.5 eV. In our case the N3 peak is accompanied by a small sharp shoulder located at 402.5 eV, which may have arisen from combination of the

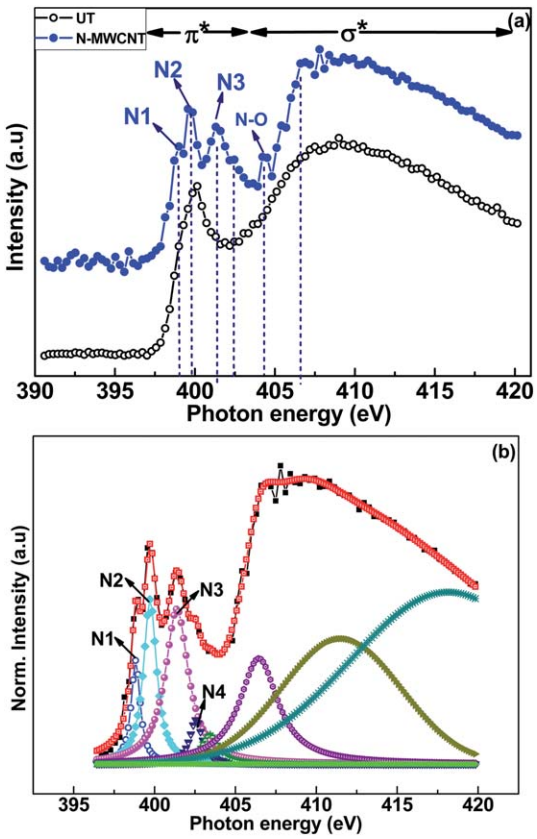

Fig. 4 (a) The N–K edge NEXAFS spectra of UT (open circles) and N-MWCNT (solid circles). The π^* peak of the N-MWCNT splits into N1, N2 and N3 corresponding to nitrogen in pyridine like sites, cyanic and graphite like, or molecular N_2. (b) The deconvolution of the N–K edge NEXAFS peak with π^* assignment.

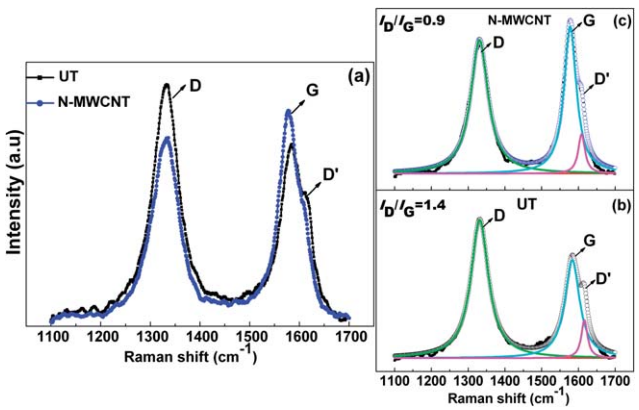

Fig. 5 (a) An overlay of the Raman D and G bands for the UT (black) and N-MWCNT (blue). (b, c) Their respective deconvolutions, fitted with two Lorentzian functions.

incorporated, molecular nitrogen and nitrogen from the graphitic sites.

Further insights of the microstructural and electronic properties of the UT and N-MWCNTs are obtained from the Raman spectroscopy as represented by Fig. 5(a, b, c). The measurements were carried out on the UT and N-MWCNTs using a LabRAM spectrometer with He–Ne (632.8 nm) laser. The spectrum of UT exhibited signature D and G band at 1332.5 and 1585 cm^{-1} respectively. It is known that the D-band is associated with series of defects: bond angle disorder, bond-length disorder and hybridisation caused by heteroatom doping such as oxygen or nitrogen and structural defects caused by high energy ion bombardment from plasma treatments.[37] In comparison with UT, the N-MWCNTs showed, a decrease in the intensity of both first order D-band and second order D band (D′), decrease in FWHM of the D band and decrease in the I_D/I_G ratio from 1.4 to 0.9 (Fig. 5(b, c)). This indicates the disordered carbon content such as the amorphous carbon and inherent defects in the structure is decreased after the N-ECR plasma treatment, which otherwise have proven to increase with other plasma methods.[18]

On the other hand G-band is related to the in-plane bond-stretching motions between pairs of sp^2-C atoms.[37–39] The intensity of the G-band increased after the N-ECR treatment, indicating an increase in the sp^2-C content. Furthermore, the redshift of the G-band to lower frequency by 5 cm^{-1} sheds deeper insight to type of doping in the CNT structure. Theoretical simulations carried for the N-doped CNTs and graphene have shown that the substitution of C with graphitic N atoms results in n-type doping, while a pyridinic and pyrrolic N atom results in p-type doping.[40–43] Recently, during synthesis of N-doped graphene by solvothermal process, Deng *et al.*, observed a red shift for the n-doped (*N*-graphite like sites) graphene and blue shift for the p-doped (pyridinic N and pyrrolic N), which agrees with the theoretical predictions.[26] The redshift (downshift) of the G-band of the N-MWNTs indicates n-type doping, which is in good concurrence with both the theoretical simulation and recent experimental results.

Previously, we have reported CNT damage (increased defects) due to the energetic ion bombardment when biasing potential of >100 V is applied during the purification of as-purchased SWCNTs (CarboLex, USA) by nitrogen RF plasma.[44] In general, ECR systems typically generate high density plasma at much lower potentials (<20 V). This can be due to, firstly, the resonance heating of electrons, which leads to relatively high degree of N_2 dissociation without significant increase in the potential or ion bombardment energies.[45,46] Secondly, the magnetic field electron confinement in the ECR configuration generates high temperature electron distribution tails (~30 eV) necessary for N_2 dissociation/ionisation.[47] During the N-ECR plasma treatment of the as-synthesised VA-MWCNTs, high flux of molecular ions of N_2 dominates the metal and amorphous carbon removal process due to highly confined dense plasma. It has been established that the nanotube tips are more reactive than the tube wall.[3] The chemical activity is enhanced due to the high flux of the molecular N_2 ions at the carbon network surrounding the metal catalyst, loosening and removing the metal catalyst particle, eventually leading to end opening (Fig. 2 (d, inset (c, d)). The dissociated nitrogen ions attach to the sidewalls, intercalates between the tubes and also incorporates into the end opened VA-MWCNT structure, leading to nitrogen doping as proven by the NEXAFS, HR-XPS and Raman analysis.

Biomedical devices constructed using the principle of nano-fluidic technology demands end opened MWCNTs having hydrophilic cavities.[48] This can be achieved using N-ECR treatment of MWCNTs, where the N-bombardment not only activates the surface creating free dangling bonds, but also actively involves in the removal of metal particles as described previously. Contact goniometric studies of N-MWCNTs revealed the switching of the surface from super hydrophobic to super hydrophilic state attributed to the dangling bonds, which acts as sites for nitrogen or oxygen attachment along with N_2 incorporation and doping. Thus, super hydrophilic N-MWCNTs facilitate their integration into many biomedical devices.

The plasma induced modification to the electronic states was demonstrated by the field emission characteristics of both UT and N-MWCNTs. FE studies were carried out with CNT samples as cathode and a tungsten tip as anode under high vacuum at room temperature. The FE characteristics are shown in Fig. 6 with the inset corresponding to Fowler-Nordheim (F–N) plot. The turn-on (E_{to}) and threshold (E_{th}) fields are defined as the electric fields required for emission current densities of 10 μA cm^{-2} and 1 mA cm^{-2} respectively.[49] The N-MWCNT samples show a low turn on field (E_{to}) 0.52 V μm^{-1} at 10 μA cm^{-2} and a threshold field (E_{th}) of 0.76 V μm^{-1} for a current density of 1 mA cm^{-2}. On the other hand, the UT nanotubes showed turn on and threshold fields of 1.24 V μm^{-1} and 1.4 V μm^{-1} much higher than the N-MWCNTs. The enhanced field emission from the N-MWCNTs is due to the removal of metal catalyst and amorphous carbon, which otherwise encapsulates the UT CNTs hindering electron emission from these sites. Nitrogen being incorporated and substituted into graphitic sites is a direct impact in the increased occupation of the π* states. Also, increase in the nitrogen concentration causes increased hopping frequency between the conduction and the valence band leading to enhanced field emission.[50] In recent reports,[25,51,52] Gui *et al.* have reported the CVD synthesised and chemically purified partially Fe filled CNTs to show very low turn on (0.24 V μm^{-1}) and threshold (0.60 V μm^{-1}) upon 60 min of nitrogen treatment owing to large amounts of defects.[51] In another instance, Ghosh

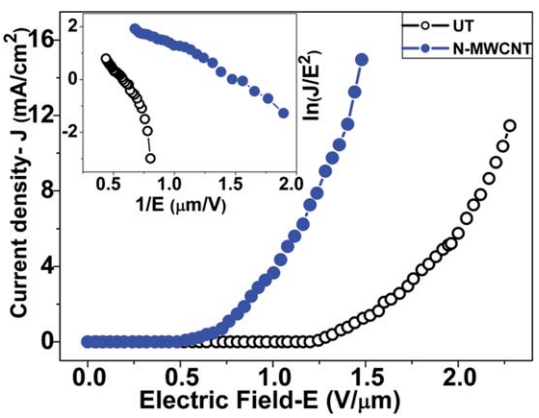

Fig. 6 J–E curves for the UT (open circles) and N-MWCNTs (solid circles). The inset shows the corresponding F–N plots.

et al., in their study of as grown, heavily doped N-CNTs, reveal a very high concentration of nitrogen (25.7 at %) to induce emission at very low fields (E_{to}-0.88 and E_{th}-2.32).[25] While, in our case the VA-MWCNTs that were N-ECR treated for mere 15 min, with relatively small amounts of nitrogen (6 at.%) exhibited very high emission current density of 15 mA cm^{-2} at very low applied voltage of 1.5 V/μm. Also, in our case the ECR treatment revealed very few or no defects confirming that the FE enhancement was due to the incorporated or attached nitrogen at specific graphite like sites.

Conclusion

A single step *in situ* growth and nitrogen ECR plasma treatment is shown to efficiently remove the metal catalyst (leading to end opening) along with amorphous carbon and successfully create n-type vertically aligned MWCNTs with complete preservation of both structure and alignment. The modification to the electronic structure was reflected in the increased π* states, where the nitrogen mostly incorporated into/intercalated between the tubes and substituted in graphite-sites as confirmed by NEXAFS, HR-XPS and Raman studies. Nitrogen incorporation pooled with removal of metal particles enhances the field emission of the CNTs resulting in high current density (15 mA cm^{-2}) at low applied voltage of 1.5 V μm^{-1} with low turn on and threshold electric fields (E_{to}-0.52 and E_{th}-0.76 V μm^{-1}). This controllable plasma treatment, which has proven to simultaneously purify, selectively modify the electronic structure for n-type and enhance surface activation has great implication in not only FE devices and bio related applications, but also many other interesting areas for cost effective energy related applications.

Acknowledgements

The author G. R. S. Iyer would like to thank the VCRS scholarship awarded by Univ. of Ulster, for pursuing her PhD., and also thank all other individuals for their useful suggestions and comments, Dr G. Beamson, NCESS, Daresbury and Dr V. Dhanak, S. R. S, Daresbury/University of Liverpool, for their help in HR-XPS and NEXAFS measurements and exciting discussions from Drs. S. S. Roy, Univ. of Ulster, S. Balaji, Univ. of Moncton, Shippagan and S. Guruvenket, Ecole Polytechnique, Montreal, Canada are greatly appreciated.

Notes and references

1 M. C. Hersam, *Nat. Nanotechnol.*, 2008, **3**, 387–394.
2 C. V. Nguyen, L. Delzeit, A. M. Cassell, J. Li, J. Han and M. Meyyappan, *Nano Lett.*, 2002, **2**, 1079–1081.
3 S. M. Huang and L. M. Dai, *J. Phys. Chem. B*, 2002, **106**, 3543–3545.
4 G. Buchs, P. Ruffieux, P. Groning and O. Groning, *Appl. Phys. Lett.*, 2007, **90**, 013104–013106.
5 K. Lee, S. C. Lim, Y. C. Choi and Y. H. Lee, *Appl. Phys. Lett.*, 2008, **93**, 063101–063103.
6 G. Y. Zhang, P. F. Qi, X. R. Wang, Y. R. Lu, D. Mann, X. L. Li and H. J. Dai, *J. Am. Chem. Soc.*, 2006, **128**, 6026–6027.
7 J. H. Cho and G. H. Kim, *Japanese Journal of Applied Physics Part 1-Regular Papers Brief Communications & Review Papers*, 2006, **45**, 8317–8322.
8 J. F. AuBuchon, L. H. Chen and S. H. Jin, *J. Phys. Chem. B*, 2005, **109**, 6044–6048.
9 W. S. Kim, J. Lee, T. W. Jeong, J. N. Heo, B. Y. Kong, Y. W. Jin, J. M. Kim, S. H. Cho, J. H. Park and D. H. Choe, *Appl. Phys. Lett.*, 2005, **87**, 163112–163114.
10 D. Wei, Y. Liu, Y. Wang, H. Zhang, L. Huang and G. Yu, *Nano Lett.*, 2009, **9**, 1752–1758.
11 C. Wang, L. Qiao, C. Qu, W. Zheng and Q. Jiang, *J. Phys. Chem. C*, 2008, **113**, 812–818.
12 A. L. M. Reddy, A. Srivastava, S. R. Gowda, H. Gullapalli, M. Dubey and P. M. Ajayan, *ACS Nano*, 2010, **4**, 6337–6342.
13 S. H. Joo, S. J. Choi, I. Oh, J. Kwak, Z. Liu, O. Terasaki and R. Ryoo, *Nature*, 2001, **412**, 169–172.
14 S. Alayoglu, A. U. Nilekar, M. Mavrikakis and B. Eichhorn, *Nat. Mater.*, 2008, **7**, 333–338.
15 J. Zhang, H. Yang, J. Fang and S. Zou, *Nano Lett.*, 2010, **10**, 638–644.
16 G. R. Li, F. Wang, Q. W. Jiang, X. P. Gao and P. W. Shen, *Angewandte Chemie International Edition*, 2010, **49**, 3653–3656.
17 L. Qu, Y. Liu, J.-B. Baek and L. Dai, *ACS Nano*, 2010, **4**, 1321–1326.
18 K. Gong, F. Du, Z. Xia, M. Durstock and L. Dai, *Science*, 2009, **323**, 760–764.
19 R. Lv, T. Cui, M. S. Jun, Q. Zhang, A. Cao, D. S. Su, Z. Zhang, S.-H. Yoon, J. Miyawaki, I. Mochida and F. Kang, *Adv. Funct. Mater.*, 2011, **21**, 999–1006.
20 J. I. B. Wilson, J. S. Walton and G. Beamson, *J. Electron Spectrosc. Relat. Phenom.*, 2001, **121**, 183–201.
21 S. S. Roy, P. Papakonstantinou, T. I. T. Okpalugo and H. Murphy, *Journal of Applied Physics*, 2006, **100**, 0537031–0537034.
22 G. Abbas, P. Papakonstantinou, G. R. S. Iyer, I. W. Kirkman and L. C. Chen, *Phys. Rev. B: Condens. Matter Mater. Phys.*, 2007, **75**, 1954291–1954299.
23 Y. Shao, S. Zhang, M. H. Engelhard, G. Li, G. Shao, Y. Wang, J. Liu, I. A. Aksay and Y. Lin, *J. Mater. Chem.*, 2010, **20**, 7491–7496.
24 H. Wang, C. Zhang, Z. Liu, L. Wang, P. Han, H. Xu, K. Zhang, S. Dong, J. Yao and G. Cui, *J. Mater. Chem.*, 2011, **21**, 5430–5434.
25 K. Ghosh, M. Kumar, T. Maruyama and Y. Ando, *J. Mater. Chem.*, 2010, **20**, 4128–4134.
26 D. H. Deng, X. L. Pan, L. A. Yu, Y. Cui, Y. P. Jiang, J. Qi, W. X. Li, Q. A. Fu, X. C. Ma, Q. K. Xue, G. Q. Sun and X. H. Bao, *Chem. Mater.*, 2011, **23**, 1188–1193.
27 L. G. Bulusheva, A. Okotrub, A. G. Kudashov, Y. V. Shubin, E. Shlyakhova, N. F. Yudanov, E. M. Pazhetnov, A. I. Boronin and D. V. Vyalikh, *Carbon*, 2008, **46**, 864–869.
28 H. C. Choi, S. Y. Bae, W. S. Jang, J. Park, H. J. Song, H. J. Shin, H. Jung and J. P. Ahn, *J. Phys. Chem. B*, 2005, **109**, 1683–1688.
29 M. Terrones, R. Kamalakaran, T. Seeger and M. Ruhle, *Chem. Commun.*, 2000, 2335–2336.
30 H. C. Choi, J. Park and B. Kim, *J. Phys. Chem. B*, 2005, **109**, 4333–4340.
31 P. Ayala, A. Grüneis, T. Gemming, D. Grimm, C. Kramberger, M. H. Rümmeli, F. L. Freire, H. Kuzmany, R. Pfeiffer, A. Barreiro, B. Büchner and T. Pichler, *J. Phys. Chem. C*, 2007, **111**, 2879–2884.
32 H. C. Choi, S. Y. Bae, J. Park, K. Seo, C. Kim, B. Kim, H. J. Song and H. J. Shin, *Appl. Phys. Lett.*, 2004, **85**, 5742–5744.
33 M. Ohkohchi, X. L. Zhao, S. Inoue and Y. Ando, *Jpn. J. Appl. Phys.*, 2004, **43**, 8365–8368.
34 A. V. Okotrub, L. G. Bulusheva, A. G. Kudashov, V. V. Belavin, D. V. Vyalikh and S. L. Molodtsov, *Appl. Phys. A: Mater. Sci. Process.*, 2009, **94**, 437–443.
35 C. Morant, R. Torres, I. Jimenez, J. M. Sanz and E. Elizalde, *J. Nanosci. Nanotechnol.*, 2009, **9**, 3633–3638.
36 S. Enouz, J. L. Bantignies, M. R. Babaa, L. Alvarez, P. Parent, F. Le Normand, O. Stephan, P. Poncharal, A. Loiseau and B. P. Doyle, *J. Nanosci. Nanotechnol.*, 2007, **7**, 3524–3527.
37 A. C. Ferrari and J. Robertson, *Phys. Rev. B: Condens. Matter*, 2000, **61**, 14095–14107.
38 A. C. Ferrari, *Solid State Commun.*, 2007, **143**, 47–57.
39 M. A. Pimenta, G. Dresselhaus, M. S. Dresselhaus, L. G. Cancado, A. Jorio and R. Saito, *Phys. Chem. Chem. Phys.*, 2007, **9**, 1276–1291.
40 H. S. Kang and S. Jeong, *Phys. Rev. B: Condens. Matter Mater. Phys.*, 2004, **70**, 233411.
41 E. Cruz-Silva, F. López-Urías, E. Muñoz-Sandoval, B. G. Sumpter, H. Terrones, J.-C. Charlier, V. Meunier and M. Terrones, *ACS Nano*, 2009, **3**, 1913–1921.
42 C. P. Ewels and M. Glerup, *J. Nanosci. Nanotechnol.*, 2005, **5**, 1345–1363.

43 E. H. Ahlgren, J. Kotakoski and A. V. Krasheninnikov, *Phys. Rev. B: Condens. Matter Mater. Phys.*, 2011, **83**, 1154241–1154247.
44 G. R. S. Iyer, P. Papakonstantinou, G. Abbas, P. D. Maguire and D. Bakirtzis, *e-J. Surf. Sci. Nanotechnol.*, 2009, **7**, 337–340.
45 H. Muta, D. H. Thang and Y. Kawai, *Surf. Coat. Technol.*, 2005, **200**, 850–854.
46 N. Itagaki, S. Iwata, K. Muta, A. Yonesu, S. Kawakami, N. Ishii and Y. Kawai, *Thin Solid Films*, 2003, **435**, 259–263.
47 T. Kaneko, S. Abe, H. Ishida and R. Hatakeyama, *Phys. Plasmas*, 2007, **14**, 110705–110707.
48 D. Tasis, N. Tagmatarchis, A. Bianco and M. Prato, *Chem. Rev.*, 2006, **106**, 1105–1136.
49 H. Zhang, D. H. Shin, H. S. Lee and C. J. Lee, *J. Phys. Chem. C*, 2007, **111**, 12954–12959.
50 Q. H. Yang, W. H. Xu, A. Tomita and T. Kyotani, *J. Am. Chem. Soc.*, 2005, **127**, 8956–8957.
51 X. C. Gui, J. Q. Wei, K. L. Wang, E. Y. Xu, R. T. Lv, D. Zhu, Z. G. Guo, F. Y. Kang, Y. Q. Zhu, D. J. Li, H. W. Zhu and D. H. Wu, *Mater. Res. Bull.*, 2010, **45**, 568–571.
52 Y. H. Lai, H. B. Lian and K. Y. Lee, *Diamond Relat. Mater.*, 2009, **18**, 544–547.

